

Uncertainty Quantification in Machine Learning for Joint Speaker Diarization and Identification

Simon W. McKnight, *Student Member, IEEE*, Aidan O. T. Hogg, *Student Member, IEEE*,
Vincent W. Neo, *Student Member, IEEE*, and Patrick A. Naylor, *Fellow, IEEE*

Abstract—This paper studies modulation spectrum features (Φ) and mel-frequency cepstral coefficients (Ψ) in joint speaker diarization and identification (JSID). JSID is important as speaker diarization on its own to distinguish speakers is insufficient for many applications, it is often necessary to identify speakers as well. Machine learning models are set up using convolutional neural networks (CNNs) on Φ and recurrent neural networks – long short-term memory (LSTMs) on Ψ , then concatenating into fully connected layers.

Experiment 1 shows machine learning models on both Φ and Ψ have significantly better diarization error rates (DERs) than models on either alone; a CNN on Φ has DER 29.09%, compared to 27.78% for a LSTM on Ψ and 19.44% for a model on both. Experiment 1 also investigates aleatoric uncertainties and shows the model on both Φ and Ψ has mean entropy 0.927 bits (out of 4 bits) for correct predictions compared to 1.896 bits for incorrect predictions which, along with entropy histogram shapes, shows the model helpfully indicates where it is uncertain.

Experiment 2 investigates epistemic uncertainties as well as aleatoric using Monte Carlo dropout (MCD). It compares models on both Φ and Ψ with models trained on x-vectors (\mathcal{X}), before applying Kalman filter smoothing on the epistemic uncertainties for resegmentation and model ensembles. While the two models on \mathcal{X} perform better (DERs 10.23% and 9.74%) than the models on Φ and Ψ (DER 17.85%) after their individual Kalman filter smoothing, combining the models using a Kalman filter smoothing method improves the DER to 9.29%. Aleatoric uncertainties are again shown to be higher for incorrect predictions.

Both Experiments show models on Φ do not distinguish overlapping speakers as well as anticipated. However, Experiment 2 shows model ensembles do better with overlapping speakers than individual models do.

Index Terms—modulation spectrum, speaker diarization, aleatoric and epistemic uncertainty, Kalman filter smoothing.

I. INTRODUCTION

SPEAKER diarization is the process of distinguishing different speakers in any given speech signal and identifying the times during which they speak. It involves two fundamental aspects: (i) segmentation of speech data into either constant time periods (e.g. a fixed number of frames) or non-constant time periods that are homogeneous in some way (e.g. single speaker speech, overlapping speaker speech or no speech); and (ii) clustering and/or labelling the segments identified to attribute them to individual speakers [1], [2], [3], [4]. Diarization is useful both alone to distinguish speakers and as an

upstream process leading to speaker identification, automatic speech recognition (ASR) or other systems.

Most diarization research systems distinguish speakers but do not identify them (e.g. as “Speaker_1”). This is consistent with diarization challenges (e.g. the DIHARD challenges [5], [6], [7]), which usually also require the system to be tested on speakers not in the training set. It is possible to have a subsequent speaker identification system that identifies speakers once they have been diarized, but a significant amount of research combines the two to, for example, improve performance or facilitate online applications. Examples include speech separation using speaker inventory [8], [9], joint speaker identification and speech separation [1] and continuous speaker identification [10]. Others reformulate as multi-label classification [11].

The term joint speaker diarization and identification (JSID) is used as the emphasis is on speaker diarization (including diarization scoring methods), but it also performs closed set speaker identification for training and testing features.

A. Modulation Spectrum Background

The modulation spectrum describes how the frequency content of a speech signal changes over time [12]. There are many different ways of calculating modulation spectrum features (Φ). This paper uses the joint acoustic and modulation spectrum approach of [13] as extended in [14]. Φ has two parts here: (i) the temporal envelope (ENV), which uses amplitude modulation (AM) principles to look at the slowly changing temporal trajectory of specific acoustic frequency bands; and (ii) the temporal fine structure (TFS), which uses frequency modulation (FM) principles to look at the rapidly changing instantaneous frequency around the centre frequencies of those acoustic frequency bands [14]. Φ is expected to perform well for distinguishing speakers [15] and detecting overlapping speakers [13].

B. Uncertainty Quantification Background

Most trained machine learning models are deterministic, with point values set for specific weights and outputs despite the inherent uncertainties caused by inaccurate labels and imperfect models. Machine learning models that additionally indicate the confidence in their predictions are generally more advantageous. Attempts have been made to quantify the levels of uncertainty [16], [17], [18], [19] in terms of: (a) aleatoric uncertainty, also known as stochastic, statistical or irreducible uncertainty; and (b) epistemic uncertainty, also known as

The authors are in the Electrical and Electronic Engineering Department, Imperial College London, Exhibition Road, South Kensington, London SW7 2BX, UK, e-mails: {s.mcknight18, a.hogg, vincent.neo09, p.naylor}@imperial.ac.uk.

This manuscript is first received 5 May 2023.

systemic or reducible uncertainty. Total uncertainty is both aleatoric and epistemic uncertainty.

Aleatoric uncertainty describes noise in observations, whereas epistemic uncertainty describes errors due to imperfect models. Epistemic uncertainty describes uncertainty in the models fitted on the data, both for the weights of the models (i.e. parametric) and the model structures. A Bayesian neural network (BNN) is a common starting point for evaluating the parametric epistemic uncertainty by fitting probability distributions for some or all of the weights in the model [20], but it was found to be very difficult to find a suitable BNN model architecture that did not underfit the data. Consequently, this paper uses the Monte Carlo dropout approximation to Bayesian inference that applies dropout during testing as well as during training [21], [22]. Note that what one machine learning model treats as aleatoric uncertainty, another may treat as epistemic uncertainty, and *vice versa* [23], [24]. Research has only recently started to investigate uncertainty quantification in speaker diarization [25], [26], and the research in those papers is very different from this research.

Aleatoric uncertainty is known to be particularly important for speaker diarization, and consequently JSID, because of the difficulty and subjectivity in obtaining accurate labels [27].

C. Resegmentation

Most diarization systems use some form of resegmentation in the post-processing stage to improve initial clusters or labels [28]. This paper considers two: simple smoothing; and Kalman filter methods, both forward only and the two-pass Rauch-Tung-Striebel (RTS) fixed interval smoothing [29].

D. This Research

The novel contributions of this research are showing that: (a) Φ and mel-frequency cepstral coefficients (MFCCs) both have information that the other does not have and establishing a model to take advantage of it; (b) aleatoric uncertainties contain meaningful information that can be used to calculate frame entropies that show how models perform based on various conditions (e.g. the number of speakers in a frame); and (c) total uncertainties can be used to combine models and improve results.

II. ANALYSIS

A. Generating Modulation Spectrum Features Φ

The 4-stage process used to generate Φ is described in [14]. Here, they are: (a) first short-time discrete Fourier transform (STFT); (b) calculate the spectral envelope using Hilbert transforms; (c) second STFT across frequency bands; and (d) calculate ENV and TFS features using Hilbert transforms.

As [14] showed that the TFS features contain additional speaker-specific information over and above the ENV features, the form of TFS features $\Phi_{TFS} \in \mathbb{R}^{L \times K \times H}$ was chosen to have the same dimensions as the ENV features $\Phi_{ENV} \in \mathbb{R}^{L \times K \times H}$ where L is the number of modulation frames, K is the number of acoustic frequency bands and H is the number of modulation frequency bands.

$\Phi \in \mathbb{R}^{L \times K \times H \times 2}$ stacks the ENV and TFS features so

$$\Phi(l, k, h, 0) = \Phi_{ENV}(l, k, h) \text{ and} \quad (1)$$

$$\Phi(l, k, h, 1) = \Phi_{TFS}(l, k, h) \quad (2)$$

for $\{l \in \mathbb{Z} : 0 \leq l \leq L - 1\}$, $\{k \in \mathbb{Z} : 0 \leq k \leq K - 1\}$ and $\{h \in \mathbb{Z} : 0 \leq h \leq H - 1\}$.

To emphasise relative magnitudes within each frame rather than absolute values, each element $\Phi_{ENV}(l, k, h)$ was divided by the Frobenius norm $\|\Phi_{ENV}(l)\|_F$ of frame l , and similarly for $\Phi_{TFS}(l)$. As is common practice, the values were then standardised across frames.

B. Uncertainty Quantification

The aleatoric uncertainty for a particular modulation frame l , speaker s of S possible speakers, input features $\mathbf{X}_{l,s}$ and output vector $\mathbf{y}_{l,s}$ where each speaker is a binary output is given by $p(\mathbf{y}_{l,s} | \mathbf{X}_{l,s}, \theta)$, where θ denotes the weights of the relevant neural network comprising the weight terms \mathbf{W} and bias terms \mathbf{b} . The epistemic uncertainty is $p(\theta | \mathcal{D}_{l,s})$, where $\mathcal{D}_{l,s}$ denotes the observed data, i.e. $\mathcal{D}_{l,s} = \{\mathbf{X}_{l,s}, \mathbf{y}_{l,s}\}$.

The experiments used Bernoulli output probability distributions following [30] to give the additional option of taking random samples from the outputs. The `IndependentBernoulli` class from the TensorFlow Probability library [31], [32] was used. However, the results reported in this paper only use the mean output, which gives exactly the same result as using sigmoid activation in the final dense layer when training with binary cross-entropy loss. In addition, it was noted that the calibration graphs such as that shown in Fig. 1 were found to be well calibrated, so no probability calibration was used.

The output aleatoric probability predicted by a particular model for a particular speaker and modulation frame is denoted by $\hat{p}(\mathbf{y}_{l,s} | \mathbf{X}_{l,s}, \theta)$ and shortened to $\hat{p}_{l,s}$. The model prediction for the speakers for that frame is then

$$\hat{y}_{l,s} = \begin{cases} 1 & \text{if } \hat{p}_{l,s} > \lambda \\ 0 & \text{if } \hat{p}_{l,s} \leq \lambda \end{cases}, \quad (3)$$

where λ is the probability threshold that is usually set to 0.5 (see Section III-G for experiments on this).

Quantifying epistemic uncertainty using Monte Carlo dropout involves running the trained model N times on the test data. As the dropout is also applied when testing, the output values differ each time, and it is then possible to fit probability distributions for the predictions of each modulation frame that would quantify the uncertainty. In this paper, the mean probability, 2.5% to 97.5% probability range, mean prediction and modal prediction are calculated. Denoting each sample n with superscript $[n]$, the mean probability is

$$\bar{p}_{l,s} = \frac{1}{N} \sum_{n=0}^{N-1} \hat{p}_{l,s}^{[n]}, \quad (4)$$

the 2.5% to 97.5% percentile probability range is calculated from those same values $\hat{p}_{l,s}^{[n]}$ sorted in ascending order and the mean prediction is

$$\bar{y}_{l,s} = \frac{1}{N} \sum_{n=0}^{N-1} \hat{y}_{l,s}^{[n]}. \quad (5)$$

Defining the set of samples for each modulation frame and speaker as $\hat{Y}_{l,s}$, the modal prediction is defined as

$$\tilde{y}_{l,s} = \arg \max_{\hat{y}_{l,s}^{[n]}} |\{\hat{y}_{l,s}^{[n]} \in \hat{Y}_{l,s}\}| \quad \forall n, \quad (6)$$

where $|\{\cdot\}|$ denotes the cardinality of the set.

Since the Kalman filter discussed in Section II-C uses standard deviations as well as means, initial experiments used the means $\bar{p}_{l,s}$ (which were generally very close to the medians) and divided the 2.5% to 97.5% percentile ranges by four to approximate the standard deviation. However, although this crude measure was a useful starting point, and better than a typical Gaussian distribution because the values of $\bar{p}_{l,s}$ were all within the range $[0, 1]$, better results were obtained by fitting a truncated Gaussian distribution $\phi_{l,s}$ instead. There is no closed-form way to calculate the values, so the distributions were fitted using the `scipy.optimize.fmin_slsqp` sequential least squares programming function on the `scipy.stats.truncnorm` generated values following [33].

C. Resegmentation

Initially, a simple smoothing mechanism was used. This had two effects: (a) it bridged prediction gaps ($\hat{y}_{l,s} = 1$ for P-MODEL and $\tilde{y}_{l,s} = 1$ for MCD-MODEL) of up to G frames, where $\{G \in \mathbb{Z} : 0 \leq G \leq 10\}$, between the same person speaking were treated as all speech; and (b) it then flattened any remaining single frame spikes. The results shown in Table V had $G = 3$. Although G was initially tested as a hyperparameter to be optimised on the validation set, the optimum value of G on the validation set did not always correspond to the optimum value of G on the test set, which led to using $G = 3$ as an empirically selected value.

An alternative method that takes advantage of the standard deviations for the epistemic uncertainty is to use Kalman filters [29]. Kalman filters work on both single models and multiple models by treating the predictions of each model as separate observations. Several variations of Kalman filters exist, but this

paper uses the two-pass RTS fixed interval method described in Algorithm 1. The Kalman filter equations are normally set out in matrix form, but since this paper is only tracking a single variable x that is based on the observations $z = \bar{p}_{l,s}$ the simpler formulation is preferred for clarity. Some experiments were also run without the backward pass step of RTS, but results were generally better with it.

The validation set was used to find optimal values of certain Kalman filter hyperparameters for subsequent use on the training set. Not all Kalman filter variable parameters were found to generalise well to the training set (e.g. the threshold percentage discussed in Section III-G), so those were set at empirically selected fixed values. Transition factor f for frame l and speaker s is

$$f_{l,s} = \begin{cases} f_0 & \text{if forward and } \bar{p}_{l,s} > \lambda \\ f_1 & \text{if forward and } \bar{p}_{l,s} \leq \lambda \\ f_2 & \text{if backward} \end{cases}, \quad (7)$$

where f_0 , f_1 and f_2 are scalars that are fitted on the validation set. Some experiments tested setting f_0 and f_1 to be the same value, but it was generally found that f_1 should be higher than f_0 . This makes sense because although f_0 bears similarities to the probability that a speaker continues speaking and f_1 to the probability that a speaker starts speaking if not speaking before, it is not exactly the same because it (a) is a multiple of the previous value of $\hat{x}_{l-1,s|l-1,s}$ and (b) could not be greater than one ($p_{l,s}$ rapidly exceeded computer memory if it did).

The process variance $q_{l,s}$ is treated similarly, though only applies in the forward stage so

$$q_{l,s} = \begin{cases} q_0 & \text{if } \bar{p}_{l,s} > \lambda \\ q_1 & \text{if } \bar{p}_{l,s} \leq \lambda \end{cases}. \quad (8)$$

The observation factor $\mathbf{h} \in \mathbb{R}^{U \times 1}$ for U models, where each h_u is fitted on the validation set. The model observation variance $R_{l,s} \in \mathbb{R}^{U \times U}$ is different for each modulation frame and is a diagonal matrix based on the epistemic uncertainty variance calculated using $\phi_{l,s}$ for each model u . The variables in Algorithm 1 are: (a) $\hat{x}_{l,s|l-1,s}$ is the initial *a priori* state estimate and $\hat{x}_{l,s|l,s}$ is the updated *a posteriori* state estimate; (b) $p_{l,s|l-1,s}$ is the initial *a priori* covariance estimate and $p_{l,s|l,s}$ is the updated *a posteriori* state estimate (i.e. it should not be confused with the use of $p_{l,s}$ for probability in Section II-B; and (c) $\mathbf{k}_{l,s} \in \mathbb{R}^{U \times 1}$ is the Kalman gain.

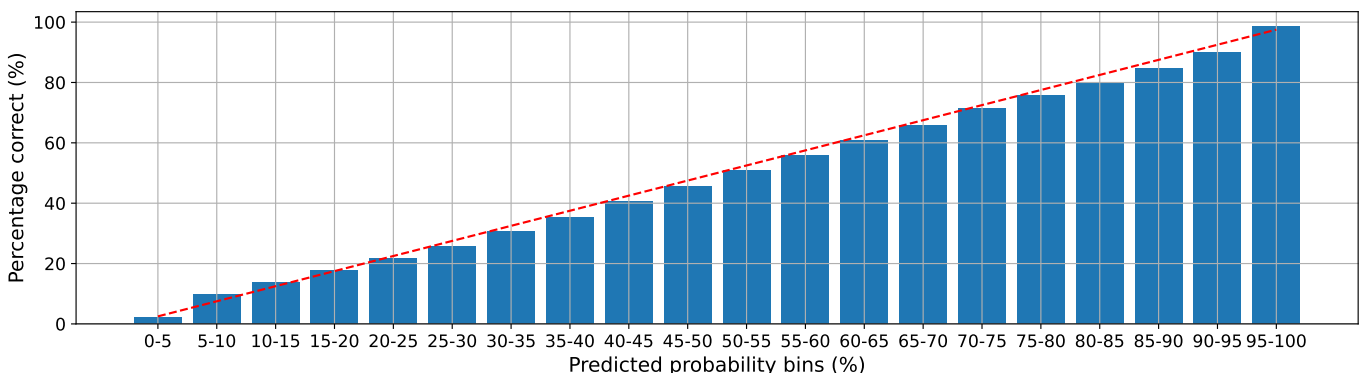


Fig. 1: Probability calibration graph on validation set for total uncertainties of MCD2- \mathcal{X}_R (defined in Section III-C).

D. Scoring Metrics

The standard binary accuracy metric in TensorFlow 2 was used on the training and validation sets, then the time-based diarization error rate (DER) metric `md-eval.pl` developed for the National Institute of Standards and Technology (NIST) Rich Transcription Challenges [34] was used on the test set. However, using the binary accuracy metric meant that a system would show around 78% accuracy simply by predicting no speakers for any frames, so the precision and recall metrics give more meaningful results.

In addition to those metrics, it became evident when running the experiments that a frame-based DER metric was essential. Although it was possible to reconstruct the signal and apply `md-eval.pl` following each training epoch, it was prohibitively computationally intensive and slow. By contrast, a frame-based DER metric could take advantage of the vectorisation and parallelisation inherent in TensorFlow 2 and its batch training, and allow easier tracking of the DER metrics during training of the models. A further benefit of a frame-based DER metric was to enable more detailed inspection of where errors occurred (e.g. whether the model tended to over- or under-estimate the number of speakers for a ground truth labelling of two or more speakers). This Section II-D describes the construction of these frame-based DER metrics.

The time-based DER metric in `md-eval.pl` is

$$DER_\tau = \frac{\tau_M + \tau_{FA} + \tau_{SE}}{\tau_{TOTAL}} = M_\tau + FA_\tau + SE_\tau, \quad (9)$$

where τ denotes time-based metrics (distinguished from ϵ used for the frame-based metrics later); $\{\tau_M, \tau_{FA}, \tau_{SE}, \tau_{TOTAL}\}$ are the missed speaker time, false alarm time, speaker error

Algorithm 1: Kalman filter tracking employed

Forward prediction

for $0 \leq s \leq S - 1$ **do**

for $0 \leq l \leq L - 1$ **do**

Predict step

$$\hat{x}_{l,s|l-1,s} = f_{l,s} \hat{x}_{l-1,s|l-1,s}$$

$$p_{l,s|l-1,s} = f_{l,s}^2 p_{l-1,s|l-1,s} + q_{l,s}$$

Update step

$$\tilde{\mathbf{y}}_{l,s} = \mathbf{z}_{l,s} - \mathbf{h} \hat{x}_{l,s|l-1,s}$$

$$\mathbf{S}_{l,s} = \mathbf{h} p_{l,s|l-1,s} \mathbf{h}^T + \mathbf{R}_{l,s}$$

$$\mathbf{k}_{l,s} = p_{l,s|l-1,s} \mathbf{h}^T \mathbf{S}_{l,s}^{-1}$$

$$\hat{x}_{l,s|l,s} = \hat{x}_{l,s|l-1,s} + \mathbf{k}_{l,s}^T \tilde{\mathbf{y}}_{l,s}$$

$$p_{l,s|l,s} = (1 - \mathbf{k}_{l,s}^T \mathbf{h}) p_{l,s|l-1,s}$$

end

end

Backward sweep

for $0 \geq s \geq S - 1$ **do**

for $L - 2 \geq l \geq 0$ **do**

$$a_{l,s} = p_{l,s|l,s} f_{l,s} / p_{l+1,s|l,s}$$

$$\hat{x}_{l,s|L-1,s} = a_{l,s} (\hat{x}_{l+1,s|L-1,s} - \hat{x}_{l+1,s|l,s})$$

$$p_{l,s|L-1,s} =$$

$$p_{l,s|l,s} + a_{l,s} (p_{l+1,s|L-1,s} - p_{l+1,s|l,s}) / a_{l,s}$$

end

end

time and total speech time respectively; and $\{M_\tau, FA_\tau, SE_\tau\}$ are the time-based missed speaker percentage, false alarm percentage and speaker error percentage respectively.

For a particular batch, the ground truth training labels $\mathbf{Y} \in \mathbb{R}^{B \times S}$, where B is the batch size, S is the number of speakers and each entry is either 0 or 1 (this is not the same as one-hot encoding as there can be more than one speaker per modulation frame). For each training batch, the miss error metric ϵ_M is calculated using

$$\epsilon_M = \frac{1}{B} \sum_{l=0}^{B-1} \max \left(\sum_{s=0}^{S-1} y_{l,s} - \sum_{s=0}^{S-1} \hat{y}_{l,s}, 0 \right) \quad (10)$$

and the false alarm metric ϵ_{FA} is calculated similarly as

$$\epsilon_{FA} = \frac{1}{B} \sum_{l=0}^{B-1} \max \left(\sum_{s=0}^{S-1} \hat{y}_{l,s} - \sum_{s=0}^{S-1} y_{l,s}, 0 \right). \quad (11)$$

The Hadamard product \odot is used to calculate $\mathbf{H} = \mathbf{Y} \odot \hat{\mathbf{Y}}$. The speaker error metric ϵ_{SE} is

$$\epsilon_{SE} = \frac{1}{B} \sum_{l=0}^{B-1} \left[\min \left(\sum_{s=0}^{S-1} \hat{y}_{l,s}, \sum_{s=0}^{S-1} y_{l,s} \right) - \sum_{s=0}^{S-1} h_{l,s} \right]. \quad (12)$$

These individual errors are summed to give ϵ_{DER} as the frame-based proxy for τ_{DER}

$$DER_\epsilon = \frac{\epsilon_M + \epsilon_{FA} + \epsilon_{SE}}{\epsilon_{TOTAL}} = M_\epsilon + FA_\epsilon + SE_\epsilon, \quad (13)$$

where ϵ denotes frame-based metrics; $\{\epsilon_M, \epsilon_{FA}, \epsilon_{SE}, \epsilon_{TOTAL}\}$ are number of missed speaker modulation frames, false alarm modulation frames, speaker error modulation frames and total speech modulation frames respectively; and $\{M_\epsilon, FA_\epsilon, SE_\epsilon\}$ are the frame-based missed speaker percentage, false alarm percentage and speaker error percentage respectively. The frame-based values do not exactly match the time-based measures because of the rounding into modulation frames as well as the use of the ground truth speech activity detection (GT-SAD) post-processing before calculating the time-based metrics.

III. EXPERIMENTAL DESIGN AND RESULTS

A. Experiment Structure

This research is split into two complementary experiments:

- 1) **Experiment 1** - studies whether modulation spectrum has useful information for speaker diarization beyond MFCCs or Ψ ; and
- 2) **Experiment 2** - studies whether total uncertainty quantification can be used to gain more meaningful information about the model predictions and produce better models in the resegmentation step.

B. Datasets and Ground Truth Labels

AMI Corpus [35] ES2008 headset recordings were used. These four meetings all had the same four speakers, which enabled (a) for Experiment 1, training on three of them and testing on one and (b) for Experiment 2, training on two of them, validating and fitting resegmentation models on one and then testing on one. Experiment 1 models were trained on

TABLE I: Statistics for ES2008 meetings, where “Dur.” is duration of meeting, “Tot. Spch” is total speech time that includes overlapping speakers individually, “Utts” is number of utterances by individual speakers, “Comb. Spch” is speech time that only counts overlapping speakers once, “Segs” is number of speech segments (one segment may have more than one speaker and more than one utterance), “Overlap” is percentage of time that there is more than one speaker, “Ch. Rate” is speaker change rate (twice number of ground truth segments divided by speech file length) and “ASD” is average segment duration.

Meeting	Dur. (mins)	Dur. (s)	Tot. Spch (s)	Utts	Comb. Spch (s)	Segs	Overlap (%)	Ch. Rate (Hz)	ASD (s)
ES2008a	17:23.360	1,043.360	806.640	168	775.940	107	3.955	0.322	4.80
ES2008b	37:11.659	2,231.659	1,849.770	439	1,742.020	248	6.185	0.393	4.21
ES2008c	35:02.621	2,102.621	1,957.110	396	1,741.850	174	12.358	0.377	4.94
ES2008d	43:45.824	2,625.824	2,349.910	757	2,113.810	396	11.169	0.577	3.10

meetings ES2008b, c and d, then tested on ES2008a as it is the shortest. Experiment 2 models use the ES2008c meetings as the validation set as it is the second shortest.

Initially, ground truth labels were constructed from the ES2008a.[A-D].segments.xml files, but it was found that (a) these contained silence of 0.25-0.5 s at the start and end of each segment [36] which greatly increased miss errors as well as confusing the model training (the reason for these silences was possibly because false positives were seen as worse than false negatives in a speech activity detection (SAD) used for ASR [37], [38]) and (b) they included non-lexical sounds such as laughter and coughing. Consequently, the ground truth labels, and also the ground truth SAD which was used in Experiment 2, were constructed from the ES2008a.[A-D].words.xml files generated for the AMI corpus for words only using forced alignment and HTK [35] (conveniently already extracted in the “only_words” directory of [39], [40]). This led to DER_e and DER_r improvements of around 6-8%. Table I shows general statistics for the meetings. Diarization performance is greatly affected by the amount of overlapping speech as well as how often the speakers change.

C. Features and Systems Used

A particular challenge for comparing single frame vector features such as MFCCs with modulation spectrum matrix features is the drastically different frame durations as well as the different shapes. MFCCs involve STFTs that need stationary processes in each frame, so the frames cannot be longer than about 40 ms [41]. By contrast, modulation spectrum features need many acoustic frames, so even if the acoustic frame steps F_a used by the modulation spectrum are significantly shorter than those for MFCCs denoted F_{a2} , using many of them will generally result in modulation frame steps F_a being significantly longer than F_{a2} . DiarTk [42] is an existing speaker diarization system that is designed to work with multiple different input feature types, but unfortunately it (a) requires different input features to have the same frame duration and step and (b) only works on vector inputs.

Consequently, a novel deep learning architecture extending [14] was established that uses convolutional neural networks (CNNs) for the modulation spectrum features and a many-to-one recurrent neural network - long short-term memory (LSTM) for a number of MFCCs such that the aggregate duration of those frame steps equals the modulation frame step. The outputs of those convolutional neural network (CNN) and LSTM blocks were then concatenated and fed into fully

connected layers. This architecture had a further benefit that it continued to work with just the CNN or LSTM blocks alone feeding into the fully connected layers. Bidirectional LSTM (BiLSTM) with output concatenation were tried in both Experiments 1 and 2, and were found to improve results in Experiment 1 but not Experiment 2.

For Experiment 1, Φ was constructed from $W_a = 3$ ms frames stepped by $F_a = 1$ ms and modulation frames $W_m = 1$ s stepped by $F_m = 250$ ms. The MFCCs Ψ were created using 30 ms frames stepped by 10 ms using 32 filter banks, reduced to 19 dimensions after the discrete cosine transform (DCT) then grouped into lots of $\frac{250}{10} = 25$ so that the aggregate length of those frame steps equals F_m .

For Experiment 2, F_m was increased to 1.5 s for consistency with the x-vector lengths in [43], [39] and which are used in Experiment 2. This enabled more direct comparison as well as facilitating the use of Kalman filters to combine the model outputs. This paper denotes x-vectors generally as \mathcal{X} . There are two types of x-vectors used in this paper, namely the 512×1 dimension x-vectors from [43] defined as \mathcal{X}_B and the 256×1 dimension x-vectors from [43] defined as \mathcal{X}_R .

The models were constructed in Python using TensorFlow 2. The TensorFlow Probability (TFP) library was used for the probabilistic layers [32]. The aleatoric aspects follow [30] and Monte Carlo dropout follows [44]. Experiments on model architecture tuning showed most consistent and reliable performance for: (a) the probabilistic model (P-MODEL) in Table II; and (b) the Monte Carlo dropout models on MFCCs and

TABLE II: P-MODEL structure (P- $\Phi\Psi$).

	Layer	Units/Filter	Activation	Output Shape
Block 1	Inputs	-	-	$(L, 25, 501, 2)$
	Conv2D	$F_1, (3, 3)$	ReLU	$(L, 23, 499, F_1)$
	Conv2D	$F_2, (3, 3)$	ReLU	$(L, 21, 497, F_2)$
	MaxPool2D	$(3, 3)$	-	$(L, 7, 165, F_2)$
	Conv2D	$F_3, (3, 3)$	ReLU	$(L, 5, 163, F_3)$
	Conv2D	$F_4, (3, 3)$	ReLU	$(L, 3, 161, F_4)$
	MaxPool2D	$(3, 3)$	-	$(L, 1, 53, F_4)$
Block 2	Flatten	-	-	$(L, 53 \times F_4)$
	Inputs	-	-	$(L, 25, 19)$
	BiLSTM	U_L	tanh/sig.	$(L, 2U_L)$
Combined	Flatten	-	-	$(L, 2U_L)$
	Concat.	-	-	$(L, 53 \times F_4 + 2U_L)$
	Dropout	-	-	-
	Dense	U_{D1}	ReLU	(L, U_{D1})
	Dropout	-	-	-
	Dense	U_{D2}	ReLU	(L, U_{D2})
	Dropout	-	-	-
Dense	S	None	(L, S)	
Bernoulli	-	-	(L, S)	

modulation spectrum features in Table III and on x-vectors in Table IV (generically referred to as the MCD-MODEL). Using P-MODEL for both modulation spectrum features is shortened to P- $\Phi\Psi$, for modulation spectrum features only (i.e. without Block 2) is shortened to P- Φ and using it without Block 1 is shortened to P- Ψ for MFCCs only, P- $\Psi\Delta$ with delta features as well and P- $\Psi\Delta\Delta$ with both delta and delta-delta features as well. Similarly, the MCD-MODEL used in Experiment 1 is shortened to MCD1- $\Phi\Psi$, shortened to MCD1- Φ without Block 2 and to MCD1- Ψ , MCD1- $\Psi\Delta$ and MCD1- $\Psi\Delta\Delta$ without Block 1 depending on the delta features included. The same logic applies to MCD2- $\Phi\Psi$, MCD2- Φ , MCD2- Ψ , MCD2- $\Psi\Delta$ and MCD2- $\Psi\Delta\Delta$.

The input data was put into batches of 512 shuffled each epoch, “valid” padding applied to the CNNs, the LSTM not stateful across modulation frames and adaptive momentum (adam) optimisation used. $N = 200$ for MCD-MODELS.

Fig. 2 shows MCD1- $\Phi\Psi$ example outputs for a 30 s test extract. The epistemic uncertainty ranges are clearly visible in parts (a) and (b), then the mean and modal predictions in (c) and (d) respectively look similar to the ground truth in (e).

Monte Carlo dropout has additional dropout layers after each CNN layer. Following [22], the LSTM has the same dropout value for the input as well as for the recurrent layers (not shown in Table IV as included in LSTM function). Importantly, dropout continued to be applied in validation and testing. In each case, the model was trained using up to 100 epochs (patience 10 and early stopping 25) and up to 100 tree Parzen estimator (TPE) trials.

Experiment 2 compares results to three baseline systems: (a) DiarTk on Ψ [42], which is a agglomerative information bottleneck system; (b) the x-vector based system in [43] (BDII); and (c) the x-vector based system in [39] (ResNet101).

D. Generating Features

Because the features are computed with different frame sizes, the relevant speech signals were prepended and appended with enough zeros before extracting the relevant features to ensure alignment. Accordingly, for a speech signal

TABLE III: MCD-MODEL structure (MCD1- $\Phi\Psi$ and MCD2- $\Phi\Psi$); “Act.” is activation, “Out. Sh.” is output shape.

	Layer	Units/Filter	Act.	MCD1 Out. Sh.	MCD2 Out. Sh.
Block 1	Inputs	-	-	$(L, 25, 501, 2)$	$(L, 25, 751, 2)$
	Conv2D	$F_1, (3, 3)$	ReLU	$(L, 23, 499, F_1)$	$(L, 23, 749, F_1)$
	Dropout	-	-	-	-
	Conv2D	$F_2, (3, 3)$	ReLU	$(L, 21, 497, F_2)$	$(L, 21, 747, F_2)$
	Dropout	-	-	-	-
	MaxPool2D	$(3, 3)$	-	$(L, 7, 165, F_2)$	$(L, 7, 249, F_2)$
	Conv2D	$F_3, (3, 3)$	ReLU	$(L, 5, 163, F_3)$	$(L, 5, 247, F_3)$
	Dropout	-	-	-	-
	Conv2D	$F_4, (3, 3)$	ReLU	$(L, 3, 161, F_4)$	$(L, 3, 245, F_4)$
	Dropout	-	-	-	-
Block 2	MaxPool2D	$(3, 3)$	-	$(L, 1, 53, F_4)$	$(1, 81, F_4)$
	Flatten	-	-	$(L, 53 \times F_4)$	$(L, 81 \times F_4)$
Block 2	Inputs	-	-	$(L, 25, 19)$	$(L, 25, 19)$
	(Bi)LSTM	U_L	tanh/sig.	$(L, 2U_L)$	(L, U_L)
Combined	Flatten	-	-	$(L, 2U_L)$	(L, U_L)
	Concat.	-	-	$(L, 53F_4 + 2U_L)$	$(L, 81F_4 + U_L)$
	Dense	U_{D1}	ReLU	(L, U_{D1})	(L, U_{D1})
	Dropout	-	-	-	-
	Dense	U_{D2}	ReLU	(L, U_{D2})	(L, U_{D2})
	Dropout	-	-	-	-
	Dense	S	None	(L, S)	(L, S)
Bernoulli	-	-	(L, S)	(L, S)	

of time duration T , the number of modulation (and x-vector) frames was $N_m = \lceil \frac{T}{F_m} \rceil$. Speech signals were prepended with $[(W_m - F_m) + (W_a - F_a)]f_s/2$ zeros and appended with $[(N_m \times F_m - T) + (W_m - F_m) + (W_a - F_a)]f_s/2$ zeros before calculating Φ and \mathcal{X} . A copy of original speech signal were prepended with $(W_{a2} - F_{a2})/2$ zeros and appended with $[(N_m \times F_m - T) + (W_{a2} - F_{a2})]f_s/2$ zeros before calculating Ψ .

Although desirable to avoid using any SAD, uncertainties around when the speech actually started meant that there were long lead-in periods that could be mitigated using a post-processing SAD, applied to the ground truth data. Furthermore, the x-vectors were trained on speech only, and therefore not trained to distinguish speech from non-speech. The frame-based error metrics are reported before this GT-SAD is performed, so only the time-based error metrics are affected by it. Note that there is a significant advantage in using a SAD as pre-processing as the system can infer at least one speaker in the relevant segment, which biases results in favour of systems using them.

E. Data Augmentation and Dither

For Experiment 2, because the size of the training was comparatively small, data augmentation was used to double the size of the training set by supplementing the clean data with features generated from the same speech files but with additive white Gaussian noise (AWGN). The noisy signal for each sample was generated using random Gaussian $\sim N(0, 1)$ and scaled to achieve the desired target signal-to-noise ratio (SNR), then added to the speech signal with values still in 16-bit wav format (i.e. before dividing by 32,768). Using 30 dB SNR, which would be almost imperceptible when listening [45], was found to improve test DER of the \mathcal{X} -based models by 1-2%, though was less helpful for the Φ -based models. Using 20 dB SNR in initial experiments made results worse in all cases, which suggests some sensitivity of the methods to noise.

Although dither was applied in the published code for generating \mathcal{X} [46], for this research dither was disappplied. Additional experiments were also carried out on Experiment 2 \mathcal{X} , Φ and Ψ to add dither (specifically a random integer in the range $[-4 : 4]$ added to the 16-bit wav speech signal), but results were not affected significantly and are not reported here.

F. Selecting Results

The experiments in this paper used the Tree Parzen Estimator (TPE) in the Hyperopt library [47], [48] to optimize the

TABLE IV: MCD2- \mathcal{X}_B and MCD2- \mathcal{X}_R .

Layer	Filter/Units	Activation	Output Shape
Inputs	-	-	$(L, [512 256], 1)$
Dense	U_{D1}	ReLU	(L, U_{D1})
Dropout	-	-	-
Dense	U_{D2}	ReLU	(L, U_{D2})
Dropout	-	-	-
Dense	U_{D3}	None	(L, S)
Bernoulli	-	-	(L, S)

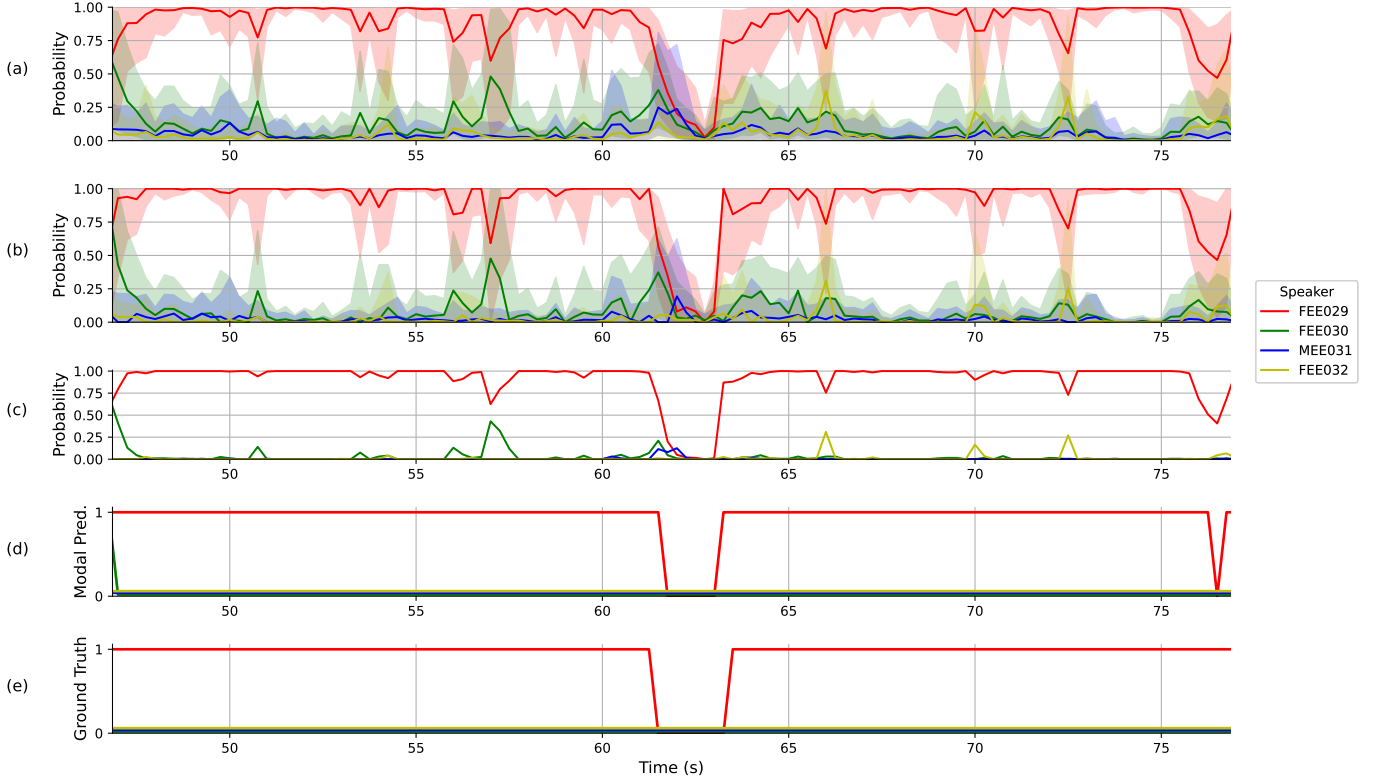


Fig. 2: 30 s extract of ES2008a for MCD1- $\Phi\Psi$ before resegmentation: (a) aleatoric uncertainty from the mean $\bar{p}_{l,s}$ and epistemic uncertainty 2.5% to 97.5% percentile range; (b) total uncertainty from fitting truncated Gaussian $\phi_{l,s}$; (c) mean prediction $\bar{y}_{l,s}$; (d) modal prediction $\hat{y}_{l,s}$; and (e) ground truth. (d) and (e) are offset slightly on y-axis to clarify overlaps. The shaded regions in (a) and (b) show the epistemic uncertainty ranges).

hyperparameters. For Experiment 1, the model with lowest DER_ϵ after each TPE trial was saved. For Experiment 2, the model from each TPE trial was then run 200 times in the Monte Carlo test simulation (applying dropout), and the modal prediction of each of the 200 modulation frames was used to calculate the final model prediction for that TPE trial. The best model retained from all TPE trials was the one that had the lowest DER_ϵ on the validation set after the Monte Carlo simulations, so models that could have had lower DER_ϵ on the test set were discarded (avoids possible overfitting).

The search space comprised the number of CNN filters in each layer ($F_1, F_2, F_3, F_4 \in \{16, 32, 64, 128\}$), the number of units in each LSTM layer ($U_L \in \{128, 256, 512\}$) and each dense layer ($U_{D1}, U_{D2} \in \{32, 64, 128, 256\}$), the dropout rates (uniform in $[0, 1]$) and the learning rate (log uniform in $[10^{-5}, 10^{-3}]$). With the LSTMs, the input dropout and

the recurrent dropout were specified to be the same value following [22]. Others that were tried were regularization rates, though later removed to rely on dropout only. It was found that the model optimization was non-convex and the random initialisation of the weights and biases had a corresponding significant impact on results. To mitigate this, the best hyperparameters for the number of CNN filters, the number of units in each LSTM layer and dense layer and the dropout rates were identified before running again with those hyperparameters fixed.

G. Threshold

Plotting the output frame-based error graphs against the prediction threshold λ in 0.1% increments consistently showed behaviour such as seen in Fig. 4, with the best test DER

TABLE V: Experiment 1 test set results comparison on best models of each type (all in %): (a) ‘‘Accu.’’ is accuracy, ‘‘Prec.’’ is precision and ‘‘Rec.’’ is recall; (b) no resegmentation applied; and (c) post-processing GT-SAD applies to time-based errors.

	Model	Accu.	Prec.	Rec.	RF1	M4	FA	SE	DER $_\epsilon$	M5	FA	SE	DER $_\epsilon$
Aleatoric	P- $\Psi\Delta$	93.42	91.71	72.34	80.88	18.52	2.28	2.76	23.55	24.33	0.00	3.25	27.58
	P- $\Psi\Delta\Delta$	93.29	92.07	71.21	80.31	19.31	1.89	2.83	24.03	25.38	0.00	3.38	28.76
	P- Φ	92.08	84.73	71.71	77.68	15.24	3.43	6.52	25.18	20.39	0.22	8.48	29.09
	P- $\Phi\Psi$	94.80	90.38	81.65	85.79	10.85	3.43	3.26	17.54	14.71	0.81	3.92	19.44
Total	MCD1- Ψ	93.47	90.46	73.83	81.30	17.06	2.92	3.07	23.05	23.15	0.24	3.49	26.88
	MCD1- $\Psi\Delta$	93.81	92.43	73.83	82.09	17.73	2.25	2.40	22.38	23.39	0.28	2.79	26.47
	MCD1- $\Psi\Delta\Delta$	93.67	91.39	74.05	81.81	17.13	2.54	2.83	22.50	22.60	0.35	3.26	26.21
	MCD1- Φ	92.57	87.08	72.02	78.84	16.22	2.92	5.29	24.44	21.50	0.32	6.93	28.75
	MCD1- $\Phi\Psi$	94.85	93.81	78.38	85.40	14.59	1.94	2.04	18.57	19.44	0.62	2.40	22.45

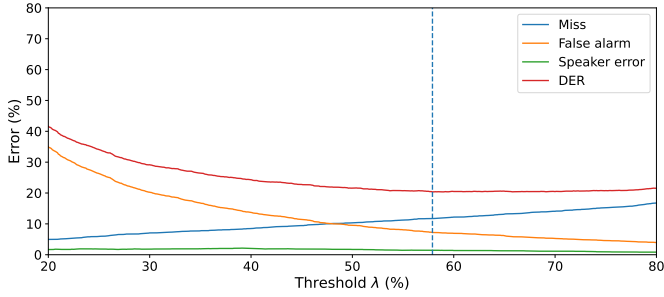


Fig. 4: Frame-based errors for threshold in 0.1% increments.

ranging from 35% to 65%. It was found that the optimum threshold for the validation set was generally not a good predictor of the optimum threshold for the test set, so it was not advantageous to include the threshold as a hyperparameter to be optimised in the TPE. Instead, λ was set at 0.5.

H. Experiment 1 Results: Ψ v Φ

Table V shows how the best performing model performed on the relevant features on which it was trained (see the “Model” columns). All models had better precision than recall, and misses were by far the largest error type. M_ϵ was generally around 60-80% of DER_ϵ and M_τ was generally around 70-90% of DER_τ (the latter is greater than the former because using the GT-SAD effectively reduces FA_τ to near zero each time, thereby increasing overall DER_τ attributable to M_τ). This shows that false negatives are more prevalent than false positives and misses are more problematic than false alarms.

The most significant result is that models using both Ψ and Φ together gives dramatically better results than either alone. This is particularly significant for the aleatoric models where P- $\Phi\Psi$ has DER_ϵ 17.54% and DER_τ 19.44% is a substantial improvement of both P- Ψ DER_ϵ 23.62% and DER_τ 27.78% and P- Φ DER_ϵ 25.18% and DER_τ 29.09%. The total uncertainty models also show significant improvements using both Ψ and Φ features, though not quite as dramatic as MCD1- $\Phi\Psi$ that has DER_ϵ 18.57% and DER_τ 22.45% improving from MCD1- Ψ DER_ϵ 23.05% and DER_τ 26.88% and MCD1- Φ DER_ϵ 24.44% and DER_τ 28.75%. There are two possible

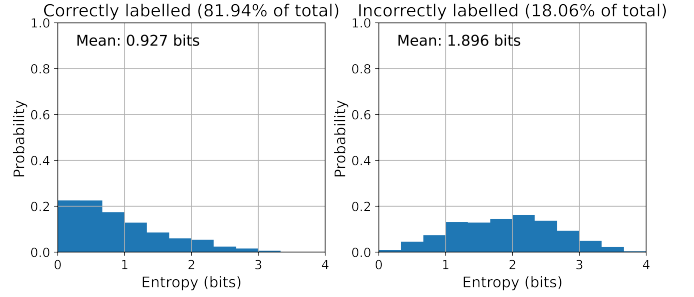


Fig. 5: Experiment 1 MCD1- $\Phi\Psi$ entropies histograms for correct and incorrect predictions of modulation frames.

conclusions to draw from this: (a) that modulation spectrum features have additional information about speaker identity that is not present in MFCCs and *vice versa*; and/or (b) the method of extracting the information using either CNN or LSTM extracts the information in a different way that effectively provides additional information about speaker identity; the CNN takes advantage of information in adjacent modulation spectrum features in through the 3×3 filters whereas the LSTM uses sequential information in the MFCCs.

Other Table V results of interest are: (a) using MFCCs on their own gives slightly better performance than Φ alone; (b) adding delta coefficients (Δ) improves results marginally, but adding delta-delta coefficients ($\Delta\Delta$) is less reliable as it sometimes improves results and sometimes does not; and (c) total uncertainty models on either Φ or Ψ alone give slightly better results than the aleatoric only models on those features, but models on both Φ and Ψ show the opposite.

Entropies for right and wrong predictions in Fig. 5 clearly show higher entropies for the wrong predictions as the mean is 0.927 bits for the correct predictions compared to 1.896 bits for the incorrect predictions. It is also evident that the shape of the correct predictions histogram is right-skewed whereas the incorrect predictions histogram is bell-shaped, which shows that in many cases the model rightly indicates that it is uncertain. There are four speakers in these files, so the maximum entropy for each modulation frame is four.

Distinguishing entropies based on the number of actual

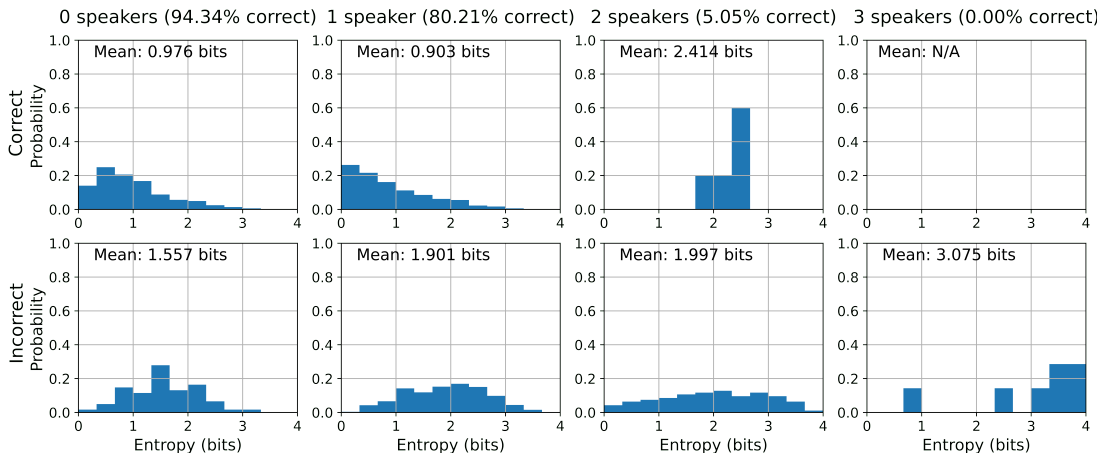


Fig. 3: Experiment 1 MCD1- $\Phi\Psi$ entropies histograms for correct and incorrect modulation frame predictions broken up by actual number of speakers in those modulation frames (none had 4 speakers).

speakers in each modulation frame as shown in Fig. 3 suggests that the modulation spectrum is not as good at distinguishing overlapping speakers as might be anticipated. For the modulation frames with 0 or 1 speaker, the means and histogram shapes for the correct predictions are similar to the correct predictions from Fig. 5, and similarly those for the incorrect predictions are similar to the incorrect predictions from Fig. 5. This is not the case with 2 speakers as the mean entropy for the correct predictions is higher than for the incorrect predictions, and many of the incorrect predictions show a high confidence (i.e. low entropy) in their results despite being incorrect. None of the modulation frames with 3 speakers were correctly predicted, and the mean entropy was high thereby correctly indicating the uncertainty. Equivalent graphs for other best performing models were found to be similar so not shown.

I. Experiment 2 Results: \mathcal{X} v Φ

The ‘‘No Reseg.’’ section of Table VI shows how the best performing model performed on the relevant data on which it was trained as specified in the ‘‘Model’’ column before any resegmentation was applied. The first three models in that section (MCD2- $\Phi\Psi$, MCD2- \mathcal{X}_B and MCD2- \mathcal{X}_R) were created for this paper. The last three are baseline models, but their respective resegmentation methods were disapplied. Fig. 6 compares a 30 s extract of each of these models, showing that the ones based on \mathcal{X} have significantly greater confidence in their predictions and will consequently dominate the Kalman filter combination, and (d) shows the Kalman filter

combination before taking the predictions based on the chosen threshold λ . Fig. 7 shows the entropies histograms for correct and incorrect predictions.

MCD2- $\Phi\Psi$ performed worse than P- $\Phi\Psi$ and MCD1- $\Phi\Psi$ from Experiment 1. Although using 1.5 s modulation frames might have been expected to give better results, here the problems were that (a) there was less training data (meeting ES2008c was used as the validation set in Experiment 2) and data augmentation was not as good a substitute and (b) the wider modulation frames meant more labelling uncertainty.

Unsurprisingly, the two models based on \mathcal{X} did better than the one based on Φ and Ψ as (a) they have the benefit of much more training data for a wider range of speakers and (b) the data is cleaner in that the speakers are clearly speaking for nearly all of the relevant frames (this is the way VoxCeleb 1 and 2 are set up, there is no timing information to consider).

As with Experiment 1, all models had better precision than recall and misses were by far the largest component of errors.

Table V compares results with the three baseline systems. In each case, the results are reported both with and without their respective in-built resegmentation methods. The baseline systems are all designed to undercluster before their resegmentation, though in the case of DiarTk and BDII the initial clustering gave good results that were subsequently made worse by the resegmentation (no change was made to the tuned hyperparameters of those systems). Each of these systems are for unsupervised speaker diarization and have a significant advantage in that they use the ground truth SAD before clustering the frames generated. Nonetheless, in general

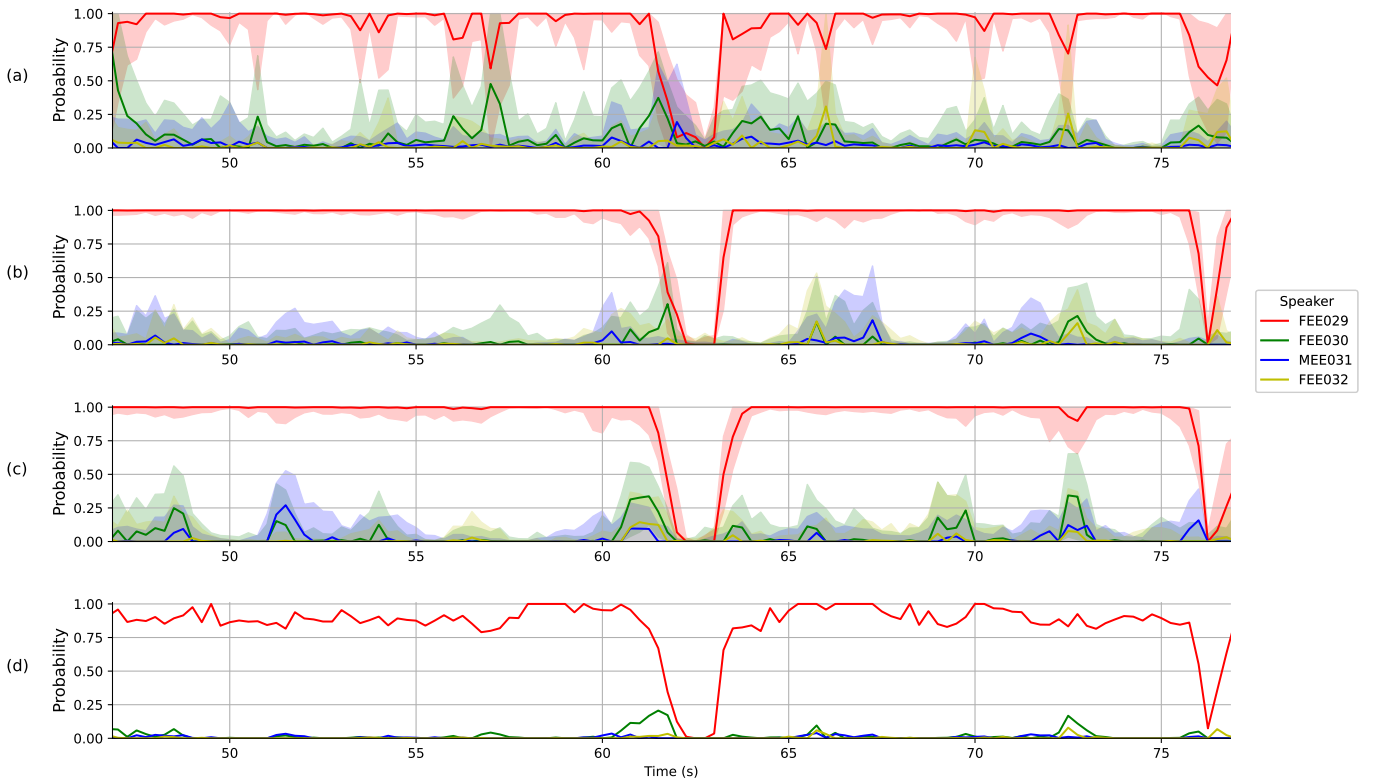


Fig. 6: Experiment 2 30 s extract of test meeting ES2008a for total uncertainty of fitting the truncated Gaussian distributions for: (a) MCD2- $\Phi\Psi$; (b) MCD2- \mathcal{X}_B ; and (c) MCD2- \mathcal{X}_R . (d) is the Kalman filter combined and smoothed version MCD2- $\Phi\Psi$, \mathcal{X}_B , \mathcal{X}_R , which only has a single aleatoric uncertainty prediction per modulation frame.

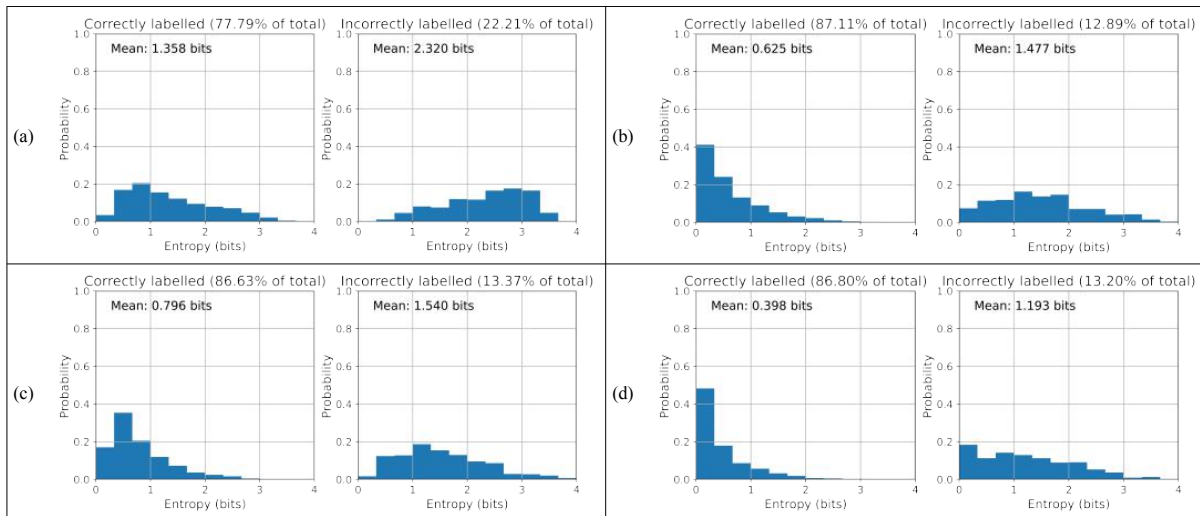


Fig. 7: Experiment 2 entropies histograms for correct and incorrect predictions of modulation frames for: (a) MCD2- $\Phi\Psi$; (b) MCD2- \mathcal{X}_B ; (c) MCD2- \mathcal{X}_R ; and (d) the Kalman filter combined and smoothed version MCD2- $\Phi\Psi$, \mathcal{X}_B , \mathcal{X}_R .

the models tested in this paper perform better than DiarTk and BDII, though not quite as well as the more recent ResNet101.

J. Experiment 2 Results: Resegmentation and Ensembles

The need for some form of resegmentation is evident when inspecting the graphical results (e.g. comparing the predictions in Fig. 2(d) with the ground truth in Fig. 2(e)) and noting the high proportion of the overall DER_ϵ and DER_τ attributable to M_ϵ and M_τ respectively in both Experiments.

Table VI in the “Smoo.” section shows how applying simple smoothing improves the results. The improvement in the frame-based measures is significant and comparable to those for Kalman filter smoothing, but the particularly good performance comes for the time-based measures. This dramatic improvement is largely attributable to the application of post-processing GT-SAD. Because the GT-SAD reduces FA_τ significantly, it will also reduce DER_τ significantly unless

M_τ and SE_τ increase significantly. M_τ and SE_τ do often increase as there is reduced speech duration to be assessed and consequently they will increase unless they are specifically improved (this is clear from Table V). By smoothing troughs of up to $G = 3$ and flattening spikes within the GT-SAD (which by definition has at least one speaker), M_τ and SE_τ turn out to be similar to M_ϵ and SE_ϵ here, thereby resulting in DER_τ being significantly better than DER_ϵ . This simple smoothing results in better performance than the DiarTk and BDII methods, but somewhat lower than ResNet101.

The results in Table VI, “KF”, show how applying Kalman filter smoothing also improves results. The frame-based metrics improve for all the single models, though most significantly for MCD2- $\Phi\Psi$ (22.42% to 19.00%) as MCD2- \mathcal{X}_B (13.49% to 12.94%), and MCD2- \mathcal{X}_R (13.94% to 13.37%) only improved marginally. Again, the improvement in time-based metrics was more substantial in all cases, with MCD2-

TABLE VI: Experiment 2 epistemic test set results comparison on best performing models of each type (all in %), where: (a) “Accu.” is accuracy, “Prec.” is precision, “Rec.” is recall; and (b) no frame-based scores available for the baseline systems.

Model	Accu.	Prec.	Rec.	F_1	M_ϵ	FA_ϵ	SE_ϵ	DER_ϵ	M_τ	FA_τ	SE_τ	DER_τ
No Reseg.	MCD2- $\Phi\Psi$	95.00	90.69	87.97	82.30	10.40	3.44	22.42	14.28	0.49	2.97	22.79
	MCD2- \mathcal{X}_B	96.44	94.13	87.89	90.91	9.06	3.69	13.49	9.30	0.66	0.88	10.84
	MCD2- \mathcal{X}_R	96.34	93.55	87.98	90.68	9.03	4.22	13.94	9.29	0.33	0.73	10.34
	DiarTk $\Psi\Delta\Delta$	-	-	-	-	-	-	-	3.80	0.00	11.39	15.33
	BDII	-	-	-	-	-	-	-	3.84	0.00	5.68	9.52
	ResNet101	-	-	-	-	-	-	-	3.84	0.00	12.26	16.10
Smoo.	MCD2- $\Phi\Psi$	95.07	93.06	81.73	87.03	13.80	3.95	0.98	18.74	14.28	1.03	1.27
	MCD2- \mathcal{X}_B	96.52	92.81	89.76	91.26	7.59	4.94	0.69	13.22	7.42	0.53	0.91
	MCD2- \mathcal{X}_R	96.42	92.02	90.11	91.06	7.23	5.61	0.72	13.61	7.22	0.27	0.71
KF	MCD2- $\Phi\Psi$	94.58	87.73	85.11	86.40	9.37	6.95	2.68	19.00	10.54	4.01	3.30
	MCD2- \mathcal{X}_B	96.54	92.02	90.79	91.40	6.56	5.49	0.89	12.94	7.10	2.02	1.11
	MCD2- \mathcal{X}_R	96.48	91.64	90.91	91.28	6.66	6.01	0.69	13.37	6.89	1.84	1.01
	MCD2- $\mathcal{X}_B, \mathcal{X}_R$	96.54	92.69	90.02	91.34	7.28	4.96	0.79	13.03	7.34	1.00	0.93
	MCD2- $\Phi\Psi, \mathcal{X}_B, \mathcal{X}_R$	96.39	91.61	90.47	91.03	6.92	5.92	0.79	13.63	6.77	1.59	0.93
Base	DiarTk $\Psi\Delta\Delta$ Viterbi	-	-	-	-	-	-	-	3.80	0.13	12.34	16.28
	BDII VBx	-	-	-	-	-	-	-	3.84	0.00	7.41	11.25
	ResNet101 VBx	-	-	-	-	-	-	-	3.84	0.00	2.39	6.23

$\Phi\Psi$ 23.79% to 17.85%, MCD2- \mathcal{X}_B 10.84% to 10.23% and 10.34% to 9.74%, albeit not as good as for simple smoothing.

The combined models MCD2- $\mathcal{X}_B, \mathcal{X}_R$ and MCD2- $\Phi\Psi, \mathcal{X}_B, \mathcal{X}_R$ do not improve the best DER_ϵ , but do improve the DER_τ . This improvement largely comes from the reduced FA_τ after applying the GT-SAD. Using the Kalman filter smoothing to combine models results in decent performance, but not as good as simple smoothing or the best baseline model. This is most likely because the models being combined are giving results that are too similar – if one had great precision and one had great recall, then combining them would make more sense than combining two with better precision than recall. A similar argument applies to misses, false alarms and speaker errors. Disappointingly, MCD2- $\Phi\Psi$ did not give the improved detection of overlapping speakers anticipated.

The entropies histograms in Fig. 7 show that MCD2- \mathcal{X}_B has the most modulation frames correct at 87.11%. This is different from the metrics in Table VI as it looks at the predictions of all speakers in the modulation frame, not summing each individually. The shape of the MCD2- \mathcal{X}_B correct predictions histogram is strongly right skewed and has a low mean of 0.625 bits that is less than half the 1.477 bits mean of the incorrect predictions. The incorrect predictions histogram is also slightly right skewed, which makes it difficult to distinguish correct and incorrect predictions based on the entropies alone. The MCD2- \mathcal{X}_R histograms and figures show similar patterns and numbers to \mathcal{X}_B , although with somewhat reduced performance. The MCD2- $\Phi\Psi$ correct predictions mean is 1.358 bits, significantly less than the 2.320 bits of the incorrect predictions, but higher than those of the other models. However, the fact that the correct predictions histogram is right skewed whereas the incorrect predictions histogram is left skewed is a significant and advantageous difference. The Kalman filter combined and smoothed model MCD2- $\Phi\Psi, \mathcal{X}_B, \mathcal{X}_R$ has 86.80% correct predictions, slightly lower than the 87.11% of MCD2- \mathcal{X}_B , but the mean entropy of the correct predictions is substantially lower at 0.398 bits compared to 0.625 bits and, importantly, is just 33.4% of the mean entropy of the correct predictions compared to 42.3% of MCD2- \mathcal{X}_B so correct predictions should be easier to distinguish from incorrect predictions. The combined model’s correct entropies histogram is more strongly right skewed than the others and its entropy information is more informative.

The entropies histograms equivalent to Fig. 3 are not reproduced for Experiment 2 for conciseness, but as in Experiment 1, the results for 0 and 1 speaker are similar to the general findings seen in Fig. 7. None of the models handled 2 speakers well. The MCD2- $\Phi\Psi$ had only 0.66% correct compared to 3.29% for MCD2- \mathcal{X}_B and 1.97% for MCD2- \mathcal{X}_R . However, the Kalman filter combined and smoothed version improved this substantially to 10.53% correct, suggesting that model ensembles should indeed help with overlapping speakers, and it also gave the highest percentage of correct frames with 1 speaker at 93.15%, though the number of correct predictions for 0 speaker frames fell substantially to 80.08%. No models correctly predicted frames with 3 speakers.

Lastly, the baselines all had much better M_τ than the MCD2-MODELS, but the latter had much better SE_τ . This

is likely because the baselines used the GT-SAD as a pre-processing step and were therefore able to infer that there was at least one speaker in the relevant segments (the M_τ were all due to missed overlapping speakers, which the baseline systems were not able to detect). By contrast, the MCD2-MODELS used GT-SAD as a post-processing step, so if they predicted a speaker when the GT-SAD said there was none then those would be removed, but predicting no speaker when the GT-SAD said there was one did not help.

IV. DISCUSSION AND CONCLUSION

Experiment 1 clearly shows that models using both Φ and Ψ are better than models using either alone for both probabilistic and Monte Carlo dropout models: (a) DER_τ is 29.09% for P1- Φ , 27.78% for P1- Ψ and 19.44% for P1- $\Phi\Psi$; and (b) DER_τ is 28.75% for MCD1- Φ , 26.88% for MCD1- Ψ and 22.45% for MCD1- $\Phi\Psi$. Experiment 1 also shows that the model on both features has mean entropy 0.927 bits (maximum 4 bits) for its correct predictions compared to 1.896 bits for its incorrect predictions, which along with the entropy histogram shapes shows the model helpfully indicates where it is uncertain.

Experiment 2 shows that models on \mathcal{X} (DER_τ is 10.23% for MCD2- \mathcal{X}_B and 9.74% for MCD2- \mathcal{X}_R) perform better than models on both Φ and Ψ (DER_τ 17.85% for MCD2- $\Phi\Psi$), in each case after their individual Kalman filter smoothing. Combining the models using a Kalman filter smoothing method improves the DER_τ to 9.29% for MCD2- $\Phi\Psi, \mathcal{X}_B, \mathcal{X}_R$, which shows it to be an advantageous way of combining models, though performance still lags behind simple smoothing of individual models (DER_τ 8.21% for MCD2- \mathcal{X}_R). The aleatoric and epistemic uncertainties are again shown to be higher for incorrect predictions.

Both Experiments 1 and 2 show that models on the modulation spectrum are not as good at distinguishing overlapping speakers as anticipated. This could be because the relevant CNN model structure is insufficient to identify the relevant relations between modulation spectrum features (only a simple 3×3 CNN filter with 4 layers is used) rather than a failing with the modulation spectrum. However, Experiment 2 shows that the combined model identifies overlapping speakers substantially better than the individual models does, though the accuracy is still poor at 10.53%.

REFERENCES

- [1] T. J. Park, N. Kanda, D. Dimitriadis, K. J. Han, S. Watanabe, and S. Narayanan, “A review of speaker diarization: recent advances with deep learning,” *Comput. Speech and Language*, vol. 72/101317, Mar. 2022.
- [2] X. Anguera Miro, S. Bozonnet, N. Evans, C. Fredouille, G. Friedland, and O. Vinyals, “Speaker diarization: a review of recent research,” *IEEE Trans. Audio, Speech, Language Process.*, vol. 20, no. 2, pp. 356–370, Feb. 2012.
- [3] S. E. Tranter and D. A. Reynolds, “An overview of automatic speaker diarization systems,” *IEEE Trans. Audio, Speech, Language Process.*, vol. 14, no. 5, pp. 1557–1565, Sep. 2006.
- [4] G. Soldi, M. Todisco, H. Delgado, C. Beaugeant, and N. Evans, “Semi-supervised on-line speaker diarization for meeting data with incremental maximum a-posteriori adaptation,” in *Proc. Odyssey: The Speaker and Language Recognition Workshop*, 2016, pp. 377–384.

- [5] N. Ryant, K. Church, C. Cieri, A. Cristia, J. Du, S. Ganapathy, and M. Liberman, "First DIHARD challenge evaluation plan," Tech. Rep., 2018. [Online]. Available: <https://zenodo.org/record/1199638#.XkABaWj7Q2w>
- [6] —, "The second DIHARD diarization challenge: dataset, task, and baselines - version 1.2," in *Proc. Conf. of Int. Speech Commun. Assoc. (INTERSPEECH)*, 2019, pp. 978–982.
- [7] N. Ryant, K. Church, C. Cieri, J. Du, S. Ganapathy, and M. Liberman, "Third DIHARD challenge evaluation plan," 2020. [Online]. Available: https://dihardchallenge.github.io/dihard3/docs/third_dihard_eval_plan_v1.2.pdf
- [8] P. Wang, Z. Chen, X. Xiao, Z. Meng, T. Yoshioka, T. Zhou, L. Lu, and J. Li, "Speech separation using speaker inventory," in *2019 IEEE Automatic Speech Recognition and Understanding Workshop (ASRU)*, Dec. 2019, pp. 230–236.
- [9] C. Han, Y. Luo, C. Li, T. Zhou, K. Kinoshita, S. Watanabe, M. Delcroix, H. Erdogan, J. R. Hershey, N. Mesgarani, and Z. Chen, "Continuous speech separation using speaker inventory for long multi-talker recording," *arXiv:2012.09727*, Dec. 2020.
- [10] N. Flemotomos and D. Dimitriadis, "A memory augmented architecture for continuous speaker identification in meetings," in *Proc. IEEE Int. Conf. on Acoust., Speech and Signal Process. (ICASSP)*, May 2020, pp. 6524–6528.
- [11] Y. Fujita, S. Watanabe, S. Horiguchi, Y. Xue, and K. Nagamatsu, "End-to-end neural diarization: reformulating speaker diarization as simple multi-label classification," *arXiv:2003.02966*, Feb. 2020.
- [12] H. Hermansky, "History of modulation spectrum in ASR," in *Proc. IEEE Int. Conf. on Acoust., Speech and Signal Process. (ICASSP)*, 2010, pp. 5458–5461.
- [13] L. Atlas and S. A. Shamma, "Joint acoustic and modulation frequency," *EURASIP J. on Advances in Signal Process.*, vol. 310290, Dec. 2003.
- [14] S. W. McKnight, A. O. T. Hogg, V. W. Neo, and P. A. Naylor, "A study of salient modulation domain features for speaker identification," in *Asia-Pacific Signal and Inform. Process. Assoc. Annual Summit and Conf. (APSIPA)*, 2021, pp. 705–712.
- [15] F.-G. Zeng, K. Nie, G. S. Stickney, Y.-Y. Kong, M. Vongphoe, A. Bhargava, C. Wei, and K. Cao, "Speech recognition with amplitude and frequency modulations," *Proc. National Academy of Sciences*, vol. 102, no. 7, pp. 2293–2298, Feb. 2005.
- [16] R. C. Smith, *Uncertainty Quantification: Theory, Implementation, and Applications*. Society for Industrial and Applied Mathematics, 2014.
- [17] R. Senge, S. Bösnér, K. Dembczyński, J. Haasenritter, O. Hirsch, N. Donner-Banzhoff, and E. Hüllermeier, "Reliable classification: learning classifiers that distinguish aleatoric and epistemic uncertainty," *Information Sciences*, vol. 255, pp. 16–29, Jan. 2014.
- [18] E. C. S. Acquesta, "Introduction to the basics of uncertainty quantification," 2019. [Online]. Available: <https://www.osti.gov/servlets/purl/1645907>
- [19] L. V. Jospin, W. Buntine, F. Boussaid, H. Laga, and M. Bennamoun, "Hands-on Bayesian neural networks – a tutorial for deep learning users," *arXiv:2007.06823*, Sep. 2021.
- [20] R. M. Neal, *Bayesian Learning for Neural Networks*, ser. Lecture Notes in Statistics, P. Bickel, P. Diggle, S. Fienberg, K. Krickeberg, I. Olkin, N. Wermuth, and S. Zeger, Eds. New York, NY: Springer New York, 1996, vol. 118.
- [21] Y. Gal and Z. Ghahramani, "Dropout as a Bayesian approximation: representing model uncertainty in deep learning," in *Proc. Int. Conf. Machine Learning (ICML)*, vol. 48, 2016, pp. 1050–1059.
- [22] Y. Gal, "Uncertainty in deep learning," Ph.D. dissertation, University of Cambridge, 2016.
- [23] A. D. Kiureghian and O. Ditlevsen, "Aleatory or epistemic? Does it matter?" *Structural Safety*, vol. 31, no. 2, pp. 105–112, Mar. 2009.
- [24] E. Hüllermeier and W. Waegeman, "Aleatoric and epistemic uncertainty in machine learning: an introduction to concepts and methods," *Machine Learning*, vol. 110, no. 3, pp. 457–506, Mar. 2021.
- [25] A. Silnova, N. Brümmer, J. Rohdin, T. Stafylakis, and L. Burget, "Probabilistic embeddings for speaker diarization," *arXiv:2004.04096*, Nov. 2020. [Online]. Available: <http://arxiv.org/abs/2004.04096>
- [26] H. Aronowitz, W. Zhu, M. Suzuki, G. Kurata, and R. Hoory, "New advances in speaker diarization," in *Proc. Conf. of Int. Speech Commun. Assoc. (INTERSPEECH)*, Oct. 2020, pp. 279–283.
- [27] S. W. McKnight, A. O. T. Hogg, and P. A. Naylor, "Analysis of phonetic dependence of segmentation errors in speaker diarization," in *Proc. Eur. Signal Process. Conf. (EUSIPCO)*, 2020.
- [28] G. Sell and D. Garcia-Romero, "Diarization resegmentation in the factor analysis subspace," in *Proc. IEEE Int. Conf. on Acoust., Speech and Signal Process. (ICASSP)*, South Brisbane, Queensland, Australia, Apr. 2015, pp. 4794–4798.
- [29] R. G. Brown and P. Y. C. Hwang, *Introduction to Random Signals and Applied Kalman Filtering with Matlab Exercises*, 4th ed. Hoboken, NJ: John Wiley & Sons, Inc., Feb. 2012.
- [30] K. Webster, "Tensorflow 2 for deep learning specialisation," 2019. [Online]. Available: <https://www.coursera.org/specializations/tensorflow2-deeplearning>
- [31] J. V. Dillon, I. Langmore, D. Tran, E. Brevdo, S. Vasudevan, D. Moore, B. Patton, A. Alemi, M. Hoffman, and R. A. Saurous, "TensorFlow Distributions," Nov. 2017. [Online]. Available: <http://arxiv.org/abs/1711.10604>
- [32] C. Davidson-Pilon, *Bayesian Methods for Hackers*, 2015. [Online]. Available: <https://camdavidsonpilon.github.io/Probabilistic-Programming-and-Bayesian-Methods-for-Hackers/#tensorflow>
- [33] scipy, "scipy.stats.truncnorm — SciPy v1.8.1 Manual." [Online]. Available: <https://docs.scipy.org/doc/scipy/reference/generated/scipy.stats.truncnorm.html>
- [34] NIST, "The 2009 (RT-09) rich transcription meeting recognition evaluation plan," Feb. 2009. [Online]. Available: https://web.archive.org/web/20100606092041if_/http://www.itl.nist.gov/iad/mig/tests/rt/2009/docs/rt09-meeting-eval-plan-v2.pdf
- [35] J. Carletta, S. Ashby, S. Bourban, M. Flynn, M. Guillelot, T. Hain, J. Kadlec, V. Karaiskos, W. Kraaij, M. Kronenthal, G. Lathoud, M. Lincoln, A. Lisowska, I. McCowan, W. Post, D. Reidsma, and P. Wellner, "The AMI meeting corpus: a pre-announcement," in *Proc. of the 2nd Int. Workshop on Mach. Learning for Multimodal Interaction (MLMI'05)*, 2006, pp. 28–39.
- [36] J. Moore, M. Kronenthal, and S. Ashby, "Guidelines for AMI speech transcriptions," Tech. Rep., 2005. [Online]. Available: <https://groups.inf.ed.ac.uk/ami/corpus/Guidelines/speech-transcription-manual.v1.2.pdf>
- [37] V. W. Neo, S. Weiss, S. W. McKnight, A. O. T. Hogg, and P. A. Naylor, "Polynomial eigenvalue decomposition-based target speaker voice activity detection in the presence of competing talkers," in *Proc. Int. Workshop on Acoustic Signal Enhancement (IWAENC)*, 2022.
- [38] J. Sohn, N. S. Kim, and W. Sung, "A statistical model-based voice activity detection," *IEEE Signal Process. Lett.*, vol. 6, no. 1, pp. 1–3, Jan. 1999.
- [39] F. Landini, J. Profant, M. Diez, and L. Burget, "Bayesian HMM clustering of x-vector sequences (VBx) in speaker diarization: theory, implementation and analysis on standard tasks," *Comput. Speech and Language*, vol. 71/101254, Dec. 2020.
- [40] —, "AMI diarization setup," 2020. [Online]. Available: <https://github.com/BUTSpeechFIT/AMI-diarization-setup>
- [41] K. K. Paliwal, J. G. Lyons, and K. K. Wojcicki, "Preference for 20-40 ms window duration in speech analysis," in *2010 4th International Conference on Signal Processing and Communication Systems*, Gold Coast, Australia, Dec. 2010, pp. 1–4.
- [42] D. Vijayasenan and F. Valente, "DiarTk: an open source toolkit for research in multistream speaker diarization and its application to meetings recordings," in *Proc. Conf. of Int. Speech Commun. Assoc. (INTERSPEECH)*, 2012, pp. 2170–2173.
- [43] F. Landini, S. Wang, M. Diez, L. Burget, P. Matějka, K. Žmolíková, L. Mošner, A. Silnova, O. Plchot, O. Novotný, H. Zeinali, and J. Rohdin, "BUT system for the second DIHARD speech diarization challenge," in *Proc. IEEE Int. Conf. on Acoust., Speech and Signal Process. (ICASSP)*, 2020, pp. 6529–6533.
- [44] O. Dürr, B. Sick, and E. Murina, *Probabilistic Deep Learning*. Manning Publications, 2020.
- [45] ICSI, "ICSI Speech FAQ - 4.1 How is the SNR of a speech example defined?" 2000. [Online]. Available: <https://www1.icsi.berkeley.edu/Speech/faq/speechSNR.html>
- [46] F. Landini and M. Diez, "VBHMM x-vectors Diarization (aka VBx)," 2020. [Online]. Available: https://github.com/BUTSpeechFIT/VBx/tree/v1.0_DIHARDII
- [47] J. Bergstra, D. Yamins, and D. D. Cox, "Making a science of model search: hyperparameter optimization in hundreds of dimensions for vision architectures," in *Proc. Int. Conf. Machine Learning (ICML)*, ser. ICML'13. Atlanta, GA, USA: JMLR.org, 2013, pp. 1–115–1–123.
- [48] F. Hutter, H. H. Hoos, and K. Leyton-Brown, "Sequential Model-Based Optimization for General Algorithm Configuration," in *Learning and Intelligent Optimization*, C. A. C. Coello, Ed. Berlin, Heidelberg: Springer Berlin Heidelberg, 2011, vol. 6683, pp. 507–523.